

# REPORT DOCUMENTATION PAGE

Public reporting burden for this collection of information is estimated to average 1 hour per response, including the time for review of the data needed, and completing and reviewing this collection of information. Send comments regarding this burden estimate or reducing this burden to Washington Headquarters Services, Directorate for Information Operations and Reports, 1215 Jefferson [Management and Budget, Paperwork Reduction Project (0704-0188), Washington, DC 20503

AFRL-SR-BL-TR-01-

ing  
or  
of

1. AGENCY USE ONLY (Leave blank)

2. REPORT DATE  
June 2001

3. REPORT TYPE A  
Final

07019

4. TITLE AND SUBTITLE

Active Damping of Resonant Modes in Unmanned Air Vehicles

5. FUNDING NUMBERS  
F49620-0001-0093

6. AUTHOR(S)

Dr. Daniel Biezad

7. PERFORMING ORGANIZATION NAME(S) AND ADDRESS(ES)

California Polytechnic State  
University  
San Luis Obispo, CA 93407

8. PERFORMING ORGANIZATION  
REPORT NUMBER  
54250/99-191

9. SPONSORING / MONITORING AGENCY NAME(S) AND ADDRESS(ES)

Air Force Office of Scientific  
Research  
Edwards AFB, CA

10. SPONSORING / MONITORING  
AGENCY REPORT NUMBER  
Project Task Number 2304/TE

11. SUPPLEMENTARY NOTES

20011220 106

12a. DISTRIBUTION / AVAILABILITY STATEMENT

Approved for public release,  
distribution unlimited

AIR FORCE OFFICE OF SCIENTIFIC RESEARCH (AFOSR)  
NOTICE OF TRANSMITTAL DTIC THIS TECHNICAL REPORT  
HAS BEEN REVIEWED AND IS APPROVED FOR PUBLIC RELEASE  
LAW AFR 190-12 DISTRIBUTION IS UNLIMITED.

12b. DISTRIBUTION CODE

13. ABSTRACT (Maximum 200 Words)

Poor handling characteristics associated with non-rigid aircraft structures can be improved by the use of an active damping system. The active system described here entails combined piezo-actuators and sensors that communicate with a processor to effectively take the structural vibration modes out of the pilot loop. The active system is integrated onto an existing simulation to predict the impact on handling qualities of an aircraft with a non-rigid structure.

The objectives of this research are to design, implement, and test active vibration controls consisting of integrated piezo actuators and sensors on flyable, scale-model aircraft. This is done to promote good handling qualities in design through an understanding of sensor dynamics and the effects of sensor and actuator location.

Methods of determining shape functions from finite-element analyses were examined and compared to wind tunnel tests. The resulting capability will allow a better prediction of the impact of structural dynamics and sensor and actuator location on the predicted stability and flight handling qualities, thus increasing both the efficiency and safety of unmanned air vehicles in flight.

14. SUBJECT TERMS

Structural Dynamics, Simulation

15. NUMBER OF PAGES  
50

16. PRICE CODE

17. SECURITY CLASSIFICATION  
OF REPORT

Unclassified

18. SECURITY CLASSIFICATION  
OF THIS PAGE

Unclassified

19. SECURITY CLASSIFICATION  
OF ABSTRACT

Unclassified

20. LIMITATION OF ABSTRACT

# **Active Damping of Resonant Modes in Unmanned Air Vehicles**

# **Final Report**

by

**Daniel J. Biezd**

**California Polytechnic State University**

**San Luis Obispo, CA. 93405**

This work is based on a thesis completed by James Bach

## **Abstract**

### **Active Damping of Resonant Modes in Unmanned Air Vehicles**

Currently, the implementation of active damping with piezoceramic actuators has been limited to flutter control at high frequencies. When an aircraft exhibits low-frequency longitudinal oscillations, the handling qualities are greatly affected. The following research provides one method for improving the longitudinal handling qualities of a non-rigid structure using digital active control.

This research entails designing, implementing, and testing active vibration controls consisting of integrated piezoceramic actuators and sensors on an unmanned model aircraft. Piezoceramic actuators and strain gages were bonded to the structure and controlled through integrated hardware and software. The vehicle is tested in Cal Poly's 3'x4' low speed wind tunnel to evaluate overall performance.

## **Acknowledgements**

This work was made possible by a grant from the United States Air Force Office of Scientific Research, award number F49620-00-1-0093, and contributions by Mr. Fred Webster and Mr. Kurt Buehler of the Air Force Flight Test Center, Edwards Air Force Base, California.

## Table of Contents

<b>List of Figures .....</b>	<b>viii</b>
<b>Nomenclature .....</b>	<b>x</b>
<b>1 Introduction .....</b>	<b>1</b>
1.1.0 Validation Methods .....	3
<b>2 Airframe Design .....</b>	<b>4</b>
2.1 Wing Design.....	5
2.2 Tail Boom Design.....	6
2.2.0 Tail Boom Sizing Parameters.....	7
<b>3 Active Control System.....</b>	<b>9</b>
3.1 Hardware .....	10
3.2 Software.....	14
<b>4 System Modeling .....</b>	<b>16</b>
4.2 Compensated Performance .....	19
4.2.0 Closed Loop Response.....	19
4.2.1 Feedback Scheme .....	20
<b>5 Impact of Sample Time on Gain Schedule.....</b>	<b>23</b>
<b>6 Experimental Setup and Procedure .....</b>	<b>26</b>
6.1 Wind Tunnel.....	26
6.2 Data Acquisition.....	27
6.3 Driving System.....	28
6.4 Active Control Architecture .....	29

6.5 Experimental Procedure .....	30
6.5.0 Wind Tunnel Velocity .....	30
6.5.1 Driving Signal Characteristics .....	31
<b>7 Results .....</b>	<b>33</b>
<b>8 Conclusion .....</b>	<b>37</b>
<b>9 References .....</b>	<b>38</b>



## List of Figures

Figure	Page
1.1 Quick pack ACX Actuator.....	2
2.1 Voltage Requirement.....	4
2.2 Aircraft Configuration.....	6
2.3 Actuator/Sensor Layout.....	8
3.1 BL1700 Microprocessor Board.....	10
3.2 PWM Hardware.....	12
3.3 XP-8910 DAC Board.....	13
3.4 Block Diagram.....	13
3.5 Programming Environment.....	14
4.1 System Model.....	16
4.2 Open Loop Performance.....	17
4.3 Modified Open Loop Response.....	18
4.4 Unity Feedback Response.....	20
4.5 System Gain Selection.....	21
4.6 Derivative Term Effect.....	22
5.1 Sample Time Effects on Response.....	23
5.2 Gain Variation with Sample Time.....	25
6.1 Wind Tunnel.....	27
6.2 LabView GUI.....	28
6.3 Active Control Signal Diagram.....	29
6.4 Unfiltered Output.....	32

Figure	Page
6.5 Filtered Output.....	33
7.1 Gain Schedules.....	33
7.2 Gyro Output.....	34
7.3 Pitch Rate Comparison.....	35
7.4 Pitch Angle Performance.....	36

## **Nomenclature**

B	Damping coefficient
DAC	Digital to Analog Converter
E	Modulus of elasticity
EPROM	Erasable Programmable Read Only Memory
F	Force, used to determine displacement, pound-force
I	Moment of inertia, in <sup>4</sup>
K	Stiffness
K <sub>D</sub>	Derivative Gain Term
K <sub>I</sub>	Integral Gain Term
K <sub>P</sub>	Proportional Gain Term
L	Length of tail boom, feet
M	Mass, pounds
P	Load, pound-force
PWM	Pulse Width Modulation
RAM	Random Access Memory
rms	Root-mean-square
X	deflection, positive defined as deflection down
$\delta$	Deflection

## **Subscripts**

D	Derivative term
I	Integrator term
P	Proportional term

## **1 Introduction**

The use of active control for stabilizing non-rigid structures along the longitudinal axis of an aircraft has been overlooked for many years. The following research presents one method for removing unnecessary longitudinal deflections with active control technology.

Active control has been investigated as a viable solution to the adverse effects of structural dynamics on aircraft for several years. The United States Navy has examined the use of piezoceramic actuators for vibration control on the F-18 fighter aircraft. The goal was to combat the excitation of the first (bending) and second (torsion) modes of the tail surfaces that result from unsteady flow impingement. The bulkhead at the base of the vertical stabilizers was cracking and breaking loose from the rest of the airframe as a result of these modes. If the deflection could be minimized, the useful life of the stabilizers and the primary structure that secures them to the aircraft could be increased (ACX).

The piezoceramic-electric actuators are thin wafer-like devices that consist of charged pieces of ceramic. The ceramic becomes rigid as a voltage is applied, creating an artificially stiff structure in the location where the actuators are bonded. Refer to Figure 1 for an illustration of the actuator.

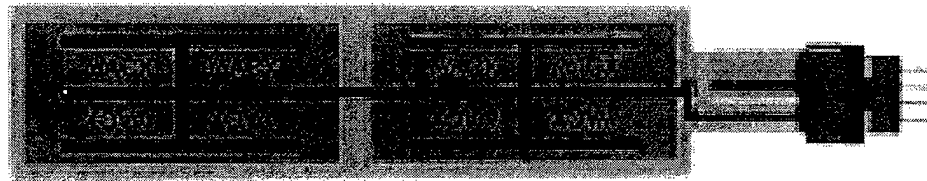


Figure 1.1 ACX QuickPack Piezoceramic Actuator

The F-18 project entailed the use of Active Control Experts (ACX) piezoceramic actuators over most of the stabilizer surface (ACX). The modifications resulted in a reduction of over 50% of the rms stress at the root of the stabilizer. This technology proved to be a viable solution to a difficult structure dynamics problem. This project presented many applications of this technology.

### **1.1 Overview**

One viable application of the active control system is the damping of the first bending mode of a non-rigid structure. Non-rigid aircraft structures can present both control lag and unpredictable/adverse flight response due to the natural bending modes of the airframe (Smith & Berry). Currently, neither flight control systems nor flight training simulations take these effects into account. The interference of these modes on pilot control can be countered by the implementation of active control. Using current technology, piezoceramic actuators can help decrease the system lag caused by non-rigid structures. By

writing the flight control software to include the active control system, it is possible to reduce the structural influence on the response of the aircraft.

The benefits of the active control system are most apparent along the longitudinal axis. Most aircraft exhibit some longitudinal deflection as a result of air loads on the tail. To better understand this problem, longitudinal structural simulations have been accomplished (Hashii, and Munger) to analyze the effects of non-rigid structure on pilot control. This work was undertaken to demonstrate and analyze the use of piezoceramic actuators for active structural compensation. For most aircraft structures, the higher frequencies usually present problems for structural engineers. Because of this, most of the focus in research has been to combat the high frequency modes. However, the normal pilot-operating regime is between one and four hertz.

To properly investigate the effects of active control on the handling qualities of an aircraft, the structure must display non-rigid qualities in the pilot's operating range. The structure is designed for the lower frequency operating range to exhibit the most impact on handling qualities.

#### *1.1.0 Validation Methods*

The active control research entails designing, testing and analysis of a vehicle that displays inadequate longitudinal rigidity. To evaluate the performance of the design approach, a small vehicle was built for testing in a low speed wind tunnel. The vehicle is outfitted with actuators and instrumentation for

analysis of the active control system. The design of the vehicle is driven by the frequency requirements, actuator size and location, and the size of the testing facility. Using LabView, a product developed by Hewlett Packard for acquiring data and testing, the performance of the active system was recorded. The complete experimental setup and testing apparatus will be discussed further in section 6 of this research paper.

## 2 Airframe Design

The primary goal of the project is to investigate the effects of a non-rigid airframe on pilot handling qualities. The airframe must exhibit longitudinal deflections large enough to introduce lag into the system. The aircraft was sized

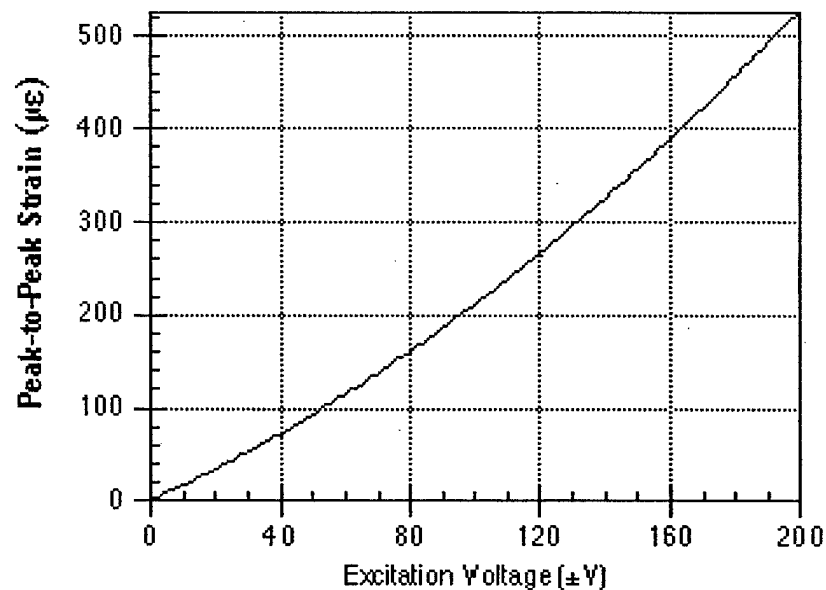


Figure 2.1 Voltage Requirement

according to the voltage required for the actuators to achieve maximum strain.

The plot in Figure 2.1 illustrates the relationship between excitation voltage (input

voltage) and strain. Notice the large voltage requirement to achieve maximum strain for the actuator. Initial sizing revealed the airplane would need to be approximately ten feet in span and almost as long. The actuator is wide, flat and rigid which drives the geometry of the fuselage to a thin, flat "tail boom."

When the aircraft is flying at any reasonable speed, the down force created by the tail would generate more strain than the actuator could output. Due to these difficulties, the flying model design was downsized to fit in Cal Poly's 3'x4' wind tunnel. Now the aircraft would have non-rigid characteristics, but on a scale that was feasible for the size of the actuator.

## ***2.1 Wing Design***

The wing pitching moment was chosen to generate a large force from the horizontal tail. The Eppler 374 was selected for its large pitching moment and very predictable stall characteristics. The plan form of the wing was optimized for minimum interference with the wall of the wind tunnel to decrease turbulence. The tunnel is four feet wide, which limited the wingspan 3.5 feet. The wing is vacuum bagged using DOW foam for the core. There is a carbon spar takes the bending loads and the torsional stiffness is achieved with fiberglass oriented on the bias. The tail was sized using historical data for both the horizontal and vertical surfaces. The tail surfaces are made of balsa with fiberglass vacuum bagged on top and bottom for added strength and durability. The configuration is illustrated in Figure 2.2.



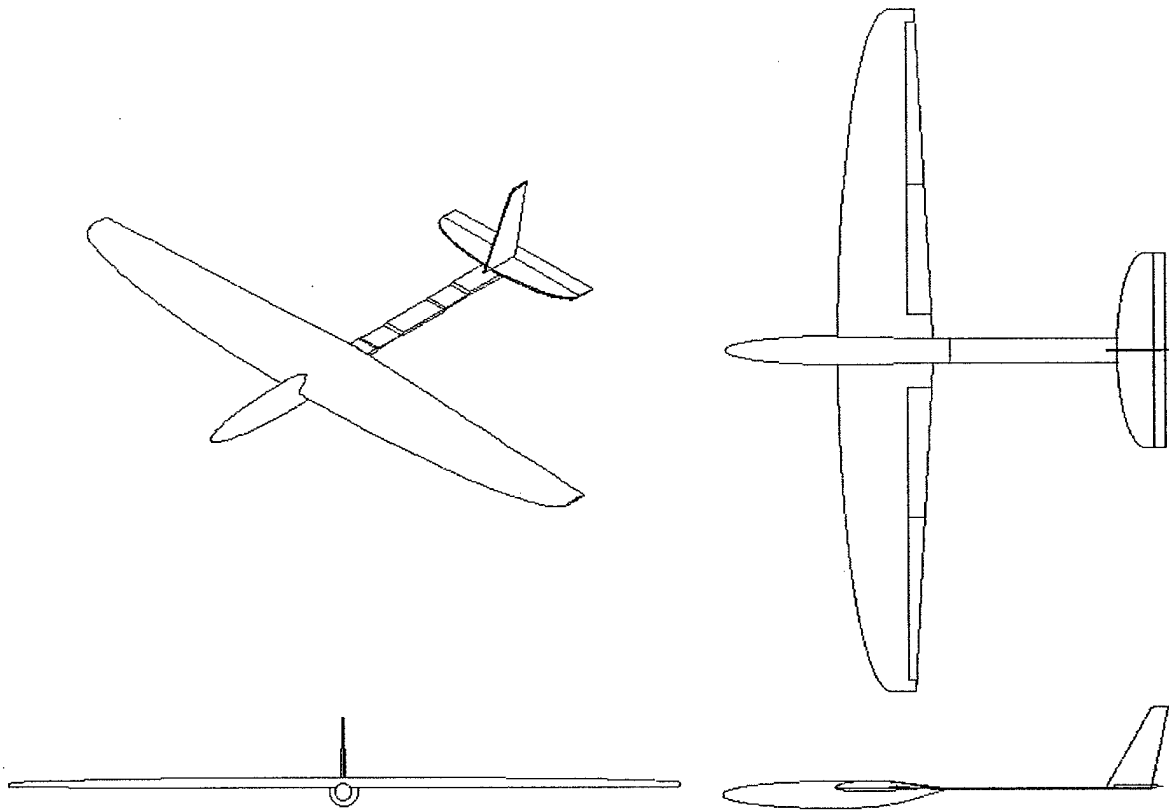


Figure 2.2 Aircraft Configuration

## 2.2 Tail Boom Design

Initially the tail boom was sized analytically using a standard beam deflection equation shown below:

$$\delta = \frac{PL^3}{6EI}$$

where  $P$  is the applied load,  $L$  is the length of the beam,  $E$  is the modulus of elasticity,  $\delta$  is the deflection in inches, and  $I$  is the moment of inertia. The tail boom length was calculated using a horizontal tail volume of 1, resulting in a

length of 18 inches. The total deflection is trivial to calculate when the cross section is constant. However, for this application the cross section changes at the location of the actuators. For this reason, the length was divided into small segments to evaluate the deflection of each segment. The thickness was optimized for a total deflection of one inch at the end. The sizing method was not easy to modify for incorporation of the actuators requiring a more detailed, higher level analysis.

The solid modeling program, SolidWorks, was used to generate a solid model of the tail boom for analysis in Cosmos/DesignStar. The forward end of the boom fixed to the fuselage was constrained in six degrees of freedom. The aft end of the boom where the tail surfaces were mounted was subjected to a downward force of half of a pound. The model was then analyzed to determine both the thickness and type of material appropriate for this application.

#### *2.2.0 Tail Boom Sizing Parameters*

The main elements directly affecting the geometry of the tail boom include; dimensions of the actuator, design natural frequency, fabrication techniques and material properties. Pilot control input is affected by structural influences at low frequencies. For this reason, the aircraft was designed for the first mode to excite between one and four Hertz. A full scale Cosmos model was created to verify the frequency domain using a vibration simulation. The shape of the tail boom was modeled with a flat thin beam configuration for several reasons: the finite element model was simplified, the actuators need a flat surface for bonding, and a wide

range of materials could be investigated for use on the model. Fiberglass has a desirable modulus of elasticity, construction characteristics, and provides significant deflection when under load. In addition, the fiberglass allowed for a variable thickness boom. Using flat molds, the tail booms was constructed to the thickness that matched the finite element model. The deflection and location of maximum strain of the structure was centralized in areas of decreased thickness. Locating the actuators on these thin sections allowed for greater actuator effectiveness. In addition, the entire boom did not have to be outfitted with costly actuators, simplifying the analysis. Refer to Figure 3 for the actuator layout. The actuators are red and the sensors are yellow. The sensors will be discussed later in the hardware section of this paper.

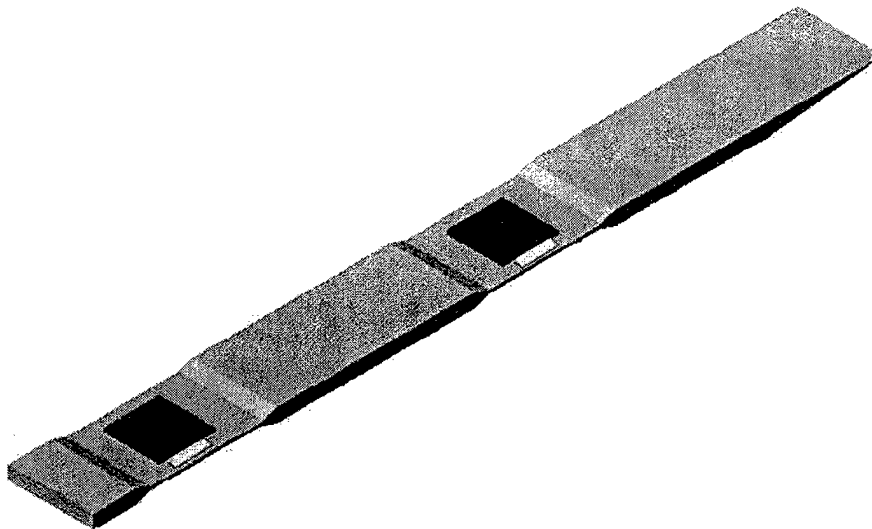


Figure 2.3 Actuator/Sensor Configuration

Strain plots proved the predictions of maximum centralized strain in the linked areas, with the strain ranging from  $300\mu\epsilon$  to  $450\mu\epsilon$ . Given this amount of strain,

the ACX manufactured, QP10N actuator was determined suitable for this application. The QP10N is a strain only, piezoceramic actuator with a maximum strain produced by the actuator of over  $500\mu\epsilon$  for a maximum excitation voltage of  $\pm 200$  volts. According to the finite element analysis, the maximum strain the links is  $500\mu\epsilon$ . Therefore, two actuators placed on both sides of the link area will provide the driving force required to sufficiently damp and stiffen each linked section of the boom.

The company specifications for the actuators state that the optimal performance occurs when the area the actuator is mounted is twice the area of the actuator itself. For an actuator that is two inches by two inches, the required area would be eight square inches. The dimensions of the links had to be modified to house the actuators. However, the natural frequency of the tail boom is greatly affected by the mass, so the area could not be increased to the full eight square inches required for optimal performance. From the ACX actuator performance plots, the QP10N would have the ability to oppose the strain produced by the force of the tail surface, even though the mounting surface was not optimal for performance.

### **3 Active Control System**

The active damping system entails two separate areas: hardware and software. The hardware enables the system to be completely digital providing real-time data acquisition and high-resolution output. The software is coded to

allow for ease of modification of the system gains. In addition, the entire system is compact and easily transferable for other applications.

### **3.1 Hardware**

The active system utilizes a combination of instrumentation and sensors that enable the processor to make real-time decisions. The heart of the active system is the Zworld BL1700 controller with a core module that includes an 18.432 MHz CPU with 32k RAM, 128k flash EPROM, and a real-time clock. The peripherals include a 12-bit analog-to-digital (A/D) converter built on to the BL1700 and a separate 12-bit digital-to-analog (D/A) converter board (Zworld XP-8910) that communicates through the PLCBus. Figure 3.1 illustrates the BL1700 board.

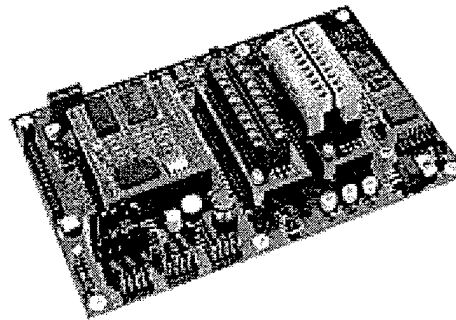


Figure 3.1 BL1700

The classic use of the ACX actuator is for both sensing and driving strain. For the steady state bending of the tail boom, the sensor must provide a constant output for optimal performance. When modeling the actuator as a sensor, the performance for the steady-state bending case resembles a capacitor. For the steady state bending application the output decays with time, providing an inaccurate sensing device. For this reason a strain gauge was used as the sensor for the input of the system.

The strain gages are bonded directly adjacent to the actuators, and are configured in a full-bridge circuit. The full bridge removes any error due to a temperature difference between the top and bottom surfaces of the tail boom. The strain gauge output is fed through an INA122 instrumentation amplifier to increase the millivolt reading from the strain gage to a useful level for the A/D converter. The amplifier gain was set with a single external resistor using the following equation

$$G = 5 + \frac{200}{R_G}$$

where  $R_G$  is the gain resistor value. The output from the strain gages is in millivolts, requiring a gain of 100 for adequate resolution into the A/D. The gain resistor value was calculated to be 21 kOhms. Due to losses and electromagnet fields, there is a small offset that was taken out in the software.

Once the deflection of the beam was measured, the signal flows from the amplifying hardware into the A/D on the main board. The A/D has 12-bits of resolution which provides the accuracy required for small beam deflections. The software generates the output through a proportional, integral derivative (PID) compensation filter before outputting to the D/A board (Z-World XP-8910).

Initially, an effort was made to utilize the Pulse Width Modulation (PWM) output on the BL1700 board to eliminate the cost of purchasing a 12-bit DAC board. The output from the PWM ranged from 0-5.73 volts. The desired output for the

filtering/amplifying hardware ranged from  $-10$  to  $+10$  volts. This output is high enough for the power amplifier that drives the actuators to work accurately. To get the 20-volt range, the gain of the amplifier needed to be about 3.5. The architecture of the PWM filter/amplifier is illustrated in Figure 3.2. Using basic electrical engineering equations, the value for the resistors was calculated as follows:

$$\frac{V_o}{V_{in}} = 1 + \frac{(R_4 + R_3)}{R_5}$$

The values of  $R_4$  and  $R_3$  (variable resistor) equal 70 kOhms to get the adjustment

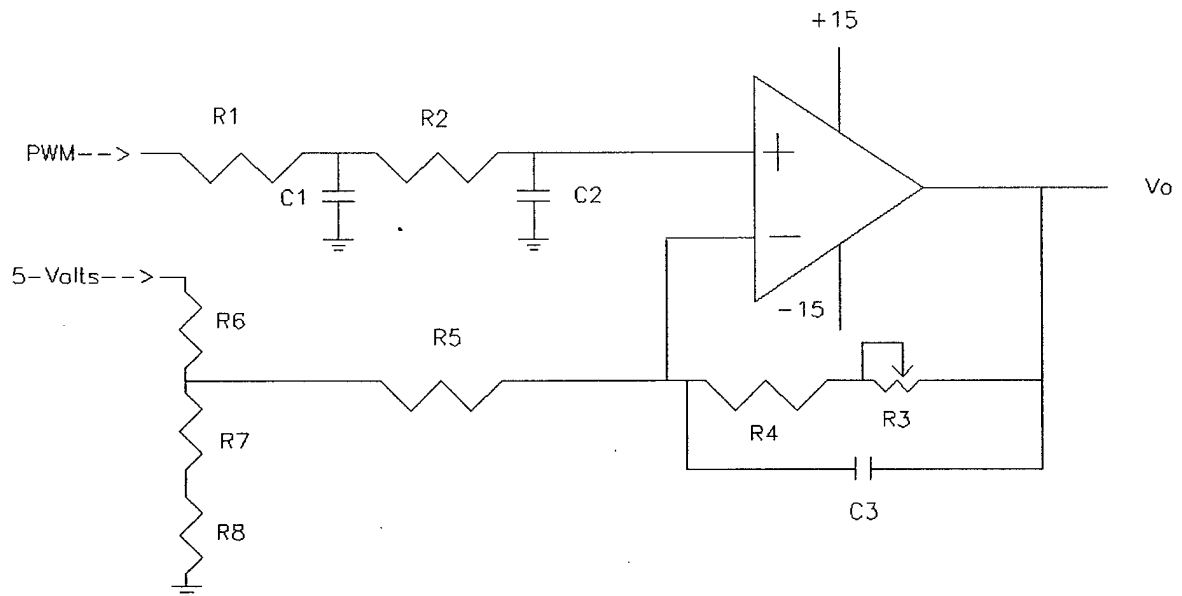


Figure 3.2 PWM Hardware

on the output required to get  $\pm 10$  volts out, and provide the ability to zero the output at steady state. Rearranging and solving for  $R_5$  yielded a value of 28 kOhms for the resistor. With the hardware assembled, the output was tested for usability. The best resolution that could be attained from the PWM was on the

order of 4 bits. Four-bit resolution is too rough to drive the actuators smoothly and additional amplifying hardware was needed for careful adjustment of the output. For this reason, a compatible DAC board (XP-8910) was purchased from Zworld to provide the resolution required for the active control system. Refer to Figure 3.3 for an illustration of the XP-8910 board.

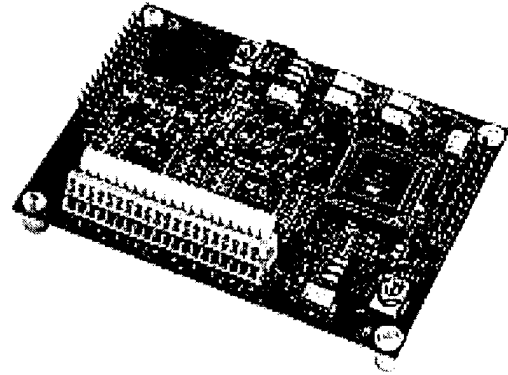


Figure 3.3 XP-8910 DAC Board

The actuators require  $\pm 200$  volts for peak strain, however the maximum output range of the D/A is  $\pm 12$  volts. Consequently, the output from the D/A is connected to a large amplifier to boost the signal to useful levels for the actuators. After the amplifier, the signal is sent to the actuators to generate the strain. A block diagram of the system is included in Figure 3.4.

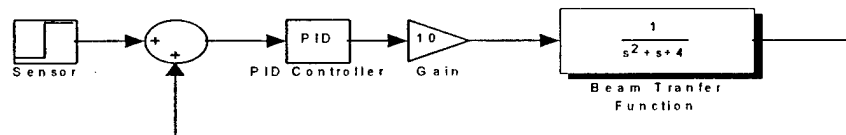
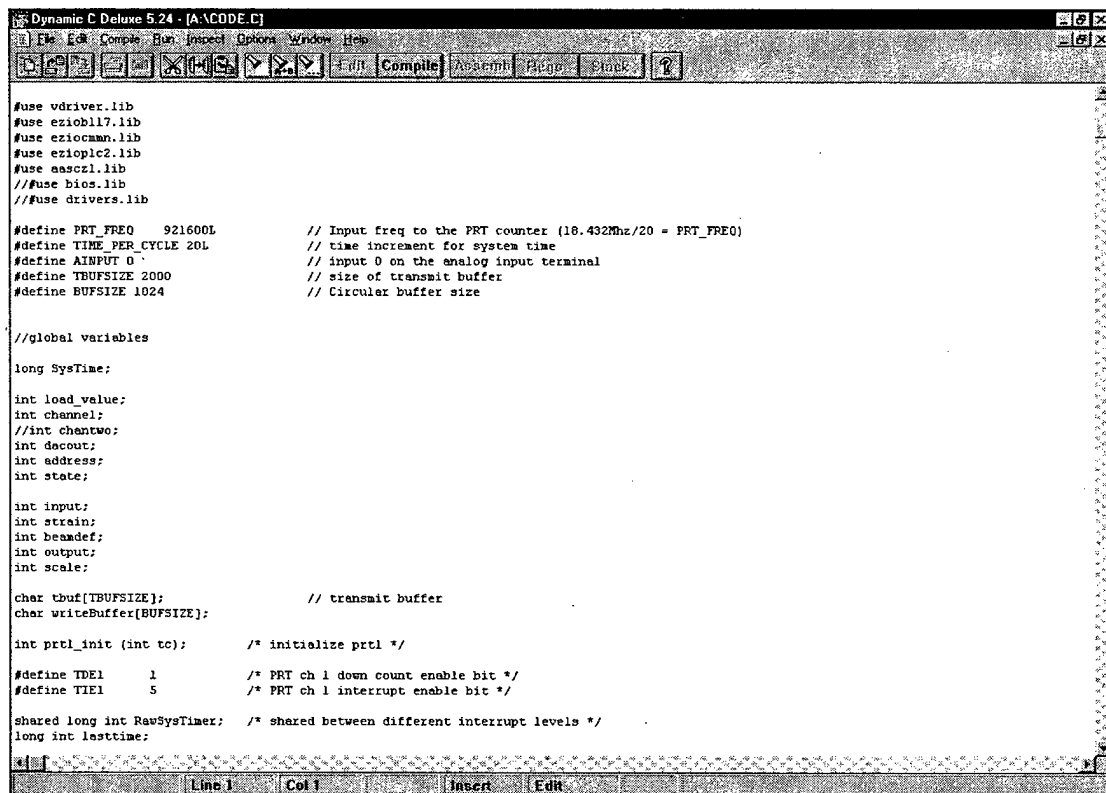


Figure 3.4 Block Diagram



### 3.2 Software

Using Dynamic C software included with the BL1700, code was written in C to drive the processor using a PID compensation loop. A sample of the interface is illustrated in Figure 3.5. The program is flashed into the EPROM by



```
Dynamic C Deluxe 5.24 - [A:\CODE.C]
File Edit Compile Run Inspect Options Window Help
[Icons] [Edit] [Compile] [Assemble] [Page] [Status] [Help]

#include <vdriver.h>
#include <ezio117.h>
#include <eziochan.h>
#include <ezioadc2.h>
#include <eziodac1.h>
#include <eziobios.h>
#include <eziodrivers.h>

#define PRT_FREQ 921600L // Input freq to the PRT counter (18.432Mhz/20 = PRT_FREQ)
#define TIME_PER_CYCLE 20L // time increment for system time
#define AINPUT 0 // input 0 on the analog input terminal
#define TBUFSIZE 2000 // size of transmit buffer
#define BUFSIZE 1024 // Circular buffer size

//global variables

long SysTime;

int load_value;
int channel;
//int chantwo;
int decout;
int address;
int state;

int input;
int strain;
int beamed;
int output;
int scale;

char tbuf[TBUFSIZE]; // transmit buffer
char writeBuffer[BUFSIZE];

int prt1_init (int tc); /* initialize prt1 */

#define TDE1 1 /* PRT ch 1 down count enable bit */
#define TIE1 5 /* PRT ch 1 interrupt enable bit */

shared long int RawSysTimer; /* shared between different interrupt levels */
long int lasttime;
```

Figure 3.5 Programming Environment

the serial link from a desktop computer to the micro controller. The program begins by calling the necessary libraries, and then proceeds with the variable declaration. The A/D converter, the bus and the D/A converter are then called for initialization. Once all the variables are initialized the data is captured from the A/D converter by the input block. After the input is scaled, the value is fed

through the processing block. All arithmetic is performed using integer mathematics to consume less processor time.

The processing block is where the PID compensation generates a new value for the output block. The initial gains were set using a simple mass spring damper system that was modeled in Matlab. The methods of modeling and an investigation of the effects of sample time on the PID gains will be discussed later in the report. The output block sends the value to the D/A converter where it's amplified and fed into the actuators.

The final block in the program is the debug block that was initially used to track the program for aid in debugging. Once the program was completed, the debug block was used as a data acquisition source to monitor the performance of the active damping system. Through the serial port on any computer, the controller can stream data real-time to a dummy terminal setup at 8 bits per second and 9600 baud. The data can then be saved and imported into a spreadsheet to determine the overall effectiveness of the control system.

Historically, the scheduling and rescheduling of the gains could take a very long time. However, with 128K EPROM the controller can be updated with new code in approximately 30 seconds. While the wind tunnel is being operated, the gains can be flashed quickly for iterating to a system that has good performance.

Refer to Appendix A for the code.

#### 4 System Modeling

Investigating the effects of an active control system requires a non-rigid body as a baseline for the analysis. The tail boom is basically a cantilevered beam with a force applied at one end that can be modeled as a mass-spring-damper system. The differential

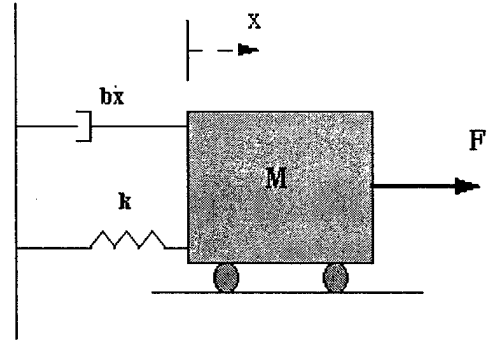


Figure 4.1 System Model

equation that describes the system is derived using the equations of motion from the free body diagram shown in Figure 4.1. Once the differential equation is determined, the LaPlace transform is taken and the transfer function becomes

$$\frac{X(s)}{F(s)} = \frac{1}{M * s^2 + b * s + k}$$

where  $M$  is the mass of the beam,  $b$  is the damping, and  $k$  is the stiffness. The stiffness of the boom was determined experimentally by observing the deflection with a one-pound weight placed at the end. The stiffness was calculated using the following equation

$$F = k * x$$

where  $F$  is the applied force and  $x$  is the distance the beam deflects. The stiffness calculated is 0.0833 lbf/ft, and the damping term was approximated

assuming 10% overshoot given a step input. These values provided a starting point for the rest of the analysis.

#### 4.1 Uncompensated Performance

Performance of the system was analyzed using Matlab. The open loop response of the system is shown in Figure 4.2. The response is typical for a second-order, over-damped system as shown with zero overshoot and a very long peak time.

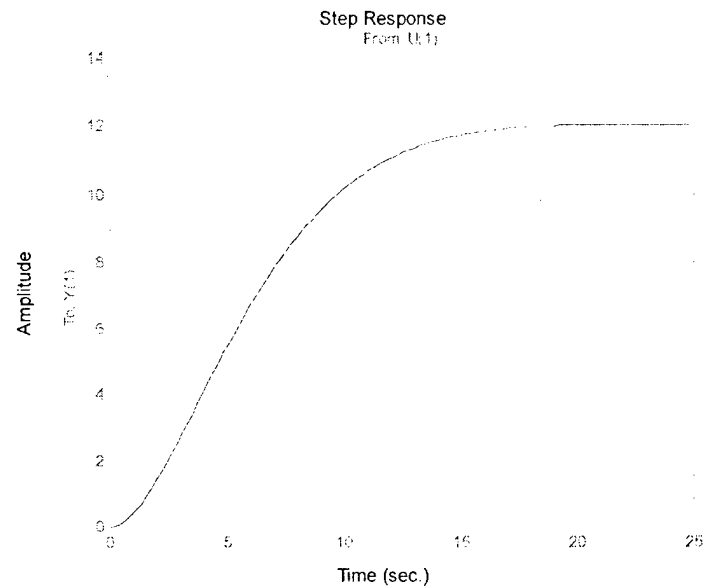


Figure 4.2 Open Loop Performance

The actual beam is much stiffer than the original prediction. Ground vibration testing (GVT) results showed the beam had a natural frequency of 2 hertz and a damping coefficient of approximately 0.25. The natural frequency of 2 hertz represents the upper limit on the bandwidth of the pilot operating range. Above 2 hertz, the pilot input becomes pure gain. These values were obtained by exciting the beam with the actuators using various input signals including chirp, sinusoid and step inputs. Values for the new transfer function that describes the beam were calculated using classical control methods (Nise). Knowing the desired natural frequency ( $\omega_n$ ) and

approximate damping coefficient ( $\zeta$ ) from the beam, the values of the transfer function were calculated using the following equations

$$b = \omega_n^2$$

$$a = 2\zeta\omega_n$$

where the transfer function is given as

$$G(s) = \frac{b}{s^2 + a*s + b}$$

The model transfer function was modified to match the beam and the open loop

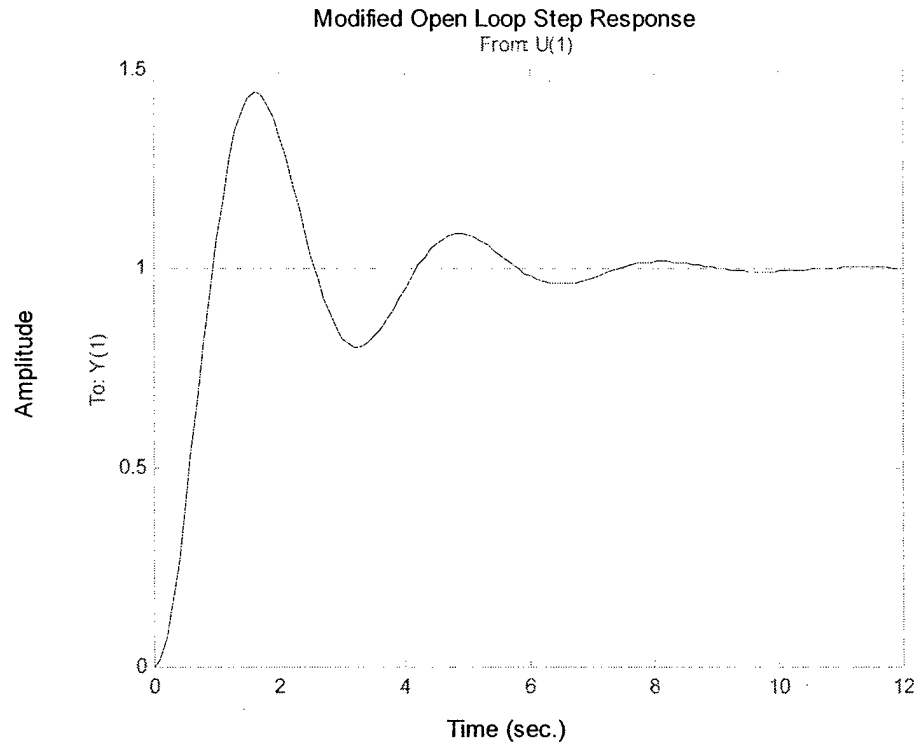


Figure 4.3 Modified Model Open Loop Response

response was changed accordingly as shown in Figure 4.3.

The performance of the uncompensated system is not desirable when designing for optimal handling qualities. If this tail boom were installed on a vehicle, the handling qualities would be very poor. For this reason, the loop on the beam is closed with a PID filter, using the ACX actuators to generate the desired response.

## ***4.2 Compensated Performance***

The goal of this research is to improve the longitudinal handling qualities of a non-rigid vehicle using active control. The model of a non-rigid structure was derived in the previous section to provide a foundation to improve upon. Introducing the piezoceramic actuators to this tail boom in a feedback scheme can take the non-rigid beam out of the pilot's operating regime.

### ***4.2.0 Closed Loop Response***

The first step is to look at the closed loop response of the baseline system. The loop is closed with unity feedback as shown in Figure 4.4. The system displays almost 50% overshoot and a peak time of over one second. This performance can easily be improved by introducing a PID compensation scheme.

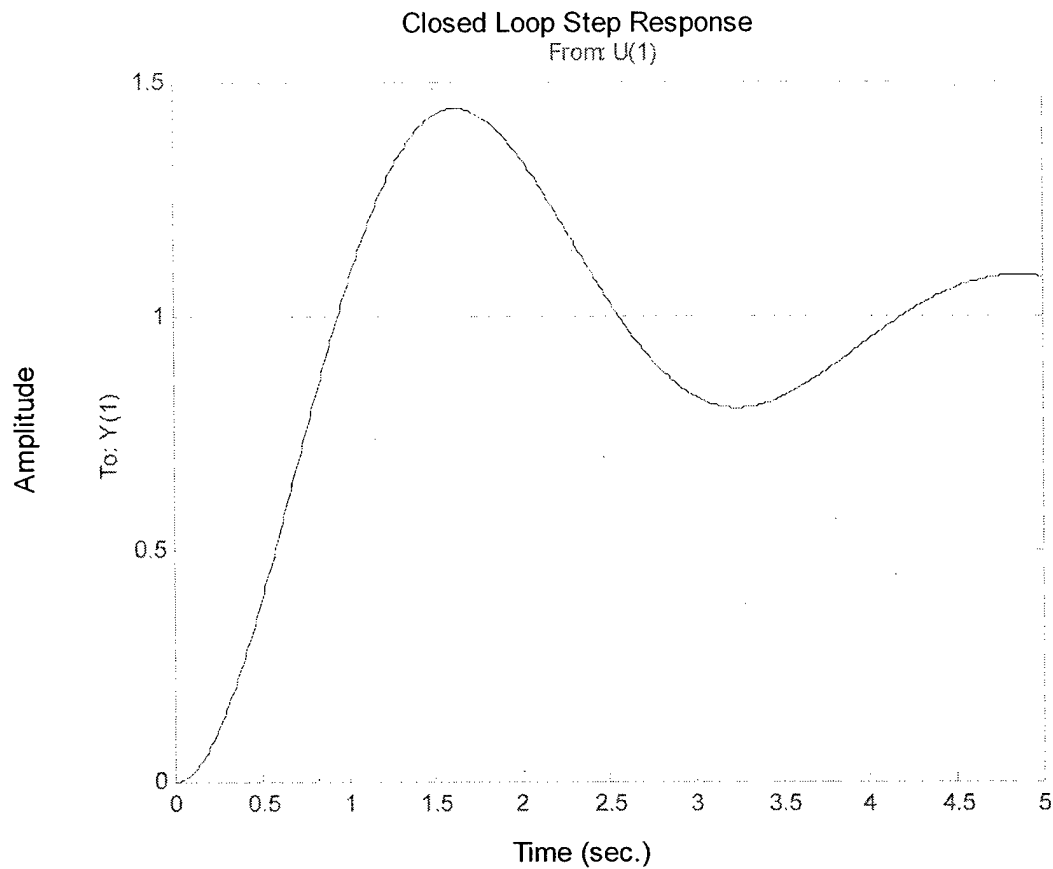


Figure 4.4 Unity Feedback Response

#### 4.2.1 Feedback Scheme

The transfer function for PID compensation is shown below

$$\frac{X(s)}{F(s)} = \frac{K_D s^2 + K_P s + K_I}{s^3 + (a + K_D)s^2 + (b + K_P)s + K_I}$$

The terms in the equation are: Proportional gain constant ( $K_P$ ), Integrator gain constant ( $K_I$ ), and Derivative gain constant ( $K_D$ ). The standard method of tuning a

system with PID control is to increase the proportional gain until the system rings. Once oscillating, the derivative term is increased to remove the overshoots that the proportional gain term caused. The integrator term is only then used if there is steady state error. Due to the natural stiffness of the beam, the system oscillates without turning the proportional gain up. However, the peak time is too long for this application, so the proportional gain was increased to drive it down. Figure 4.5 shows the results after adding proportional gain of 10.

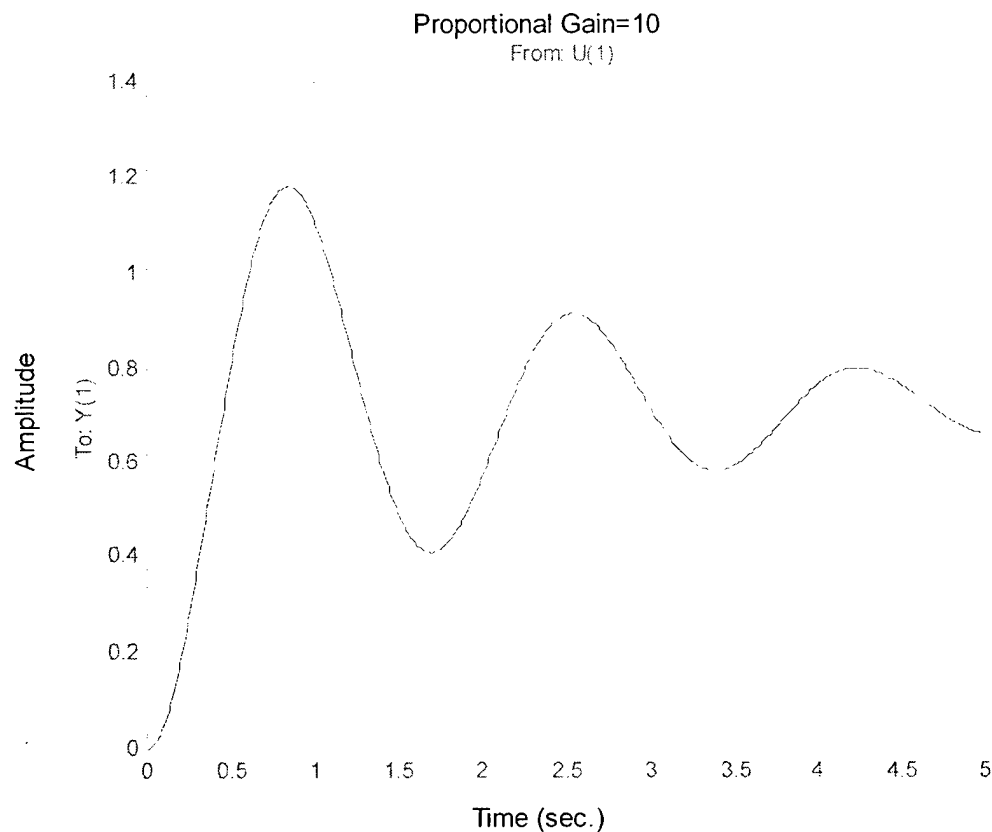


Figure 4.5 System Gain Selection

The large overshoots can be removed with a derivative term that compares the rate of change of the error to the current position and modifies the response.



The results of adding a derivative gain of 5 are illustrated in Figure 4.6. The first overshoot is inherent in the system, but the rest were removed by the derivative term.

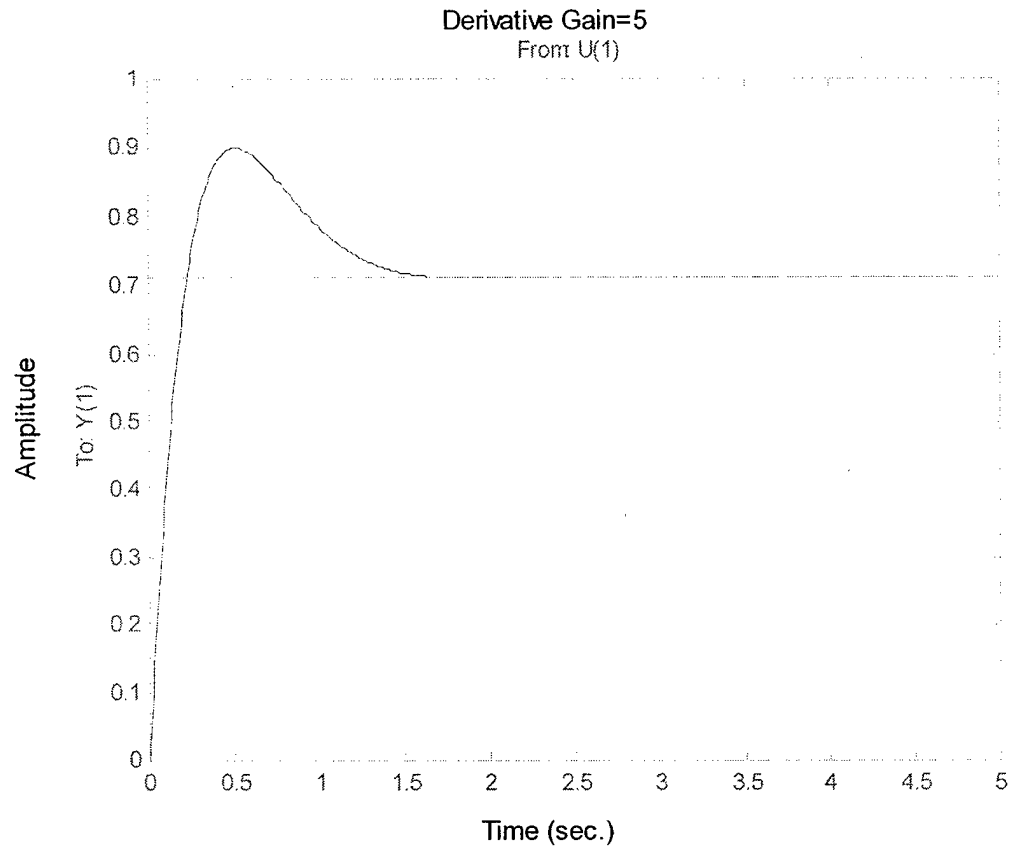


Figure 4.6 Derivative Term Effects

For this application, the steady-state error is not evident in the model so the integrator gain is left at zero. The integrator term is left in the model in case the actual boom does have steady-state error.

#### 4.2.2 Integrator

Assuming the horizontal tail is capable of generating a one-pound force, the beam should deflect approximately one inch. This deflection causes a change in angle of attack at the tail large enough to allow the airplane to “tuck” at high speeds. The tucking occurs because at the critical angle of attack, the tail begins to generate lift in the same direction as the wing. This will only occur at high speeds where the tail load is very large. The integrator term could eliminate the tendency for the airplane to tuck. The gain will be set when the vehicle is in the tunnel during the experiment.

### 5 Impact of Sample Time on Gain Schedule

The close relationship of the system sampling time and PID gains becomes very obvious when the sample time is decreased significantly. When increasing the sample time, lag is immediately introduced into the system. Figure 5.1 illustrates this correlation.

The goal of this investigation is to determine an algorithm that scales the gains with sample time to achieve the same system performance for a

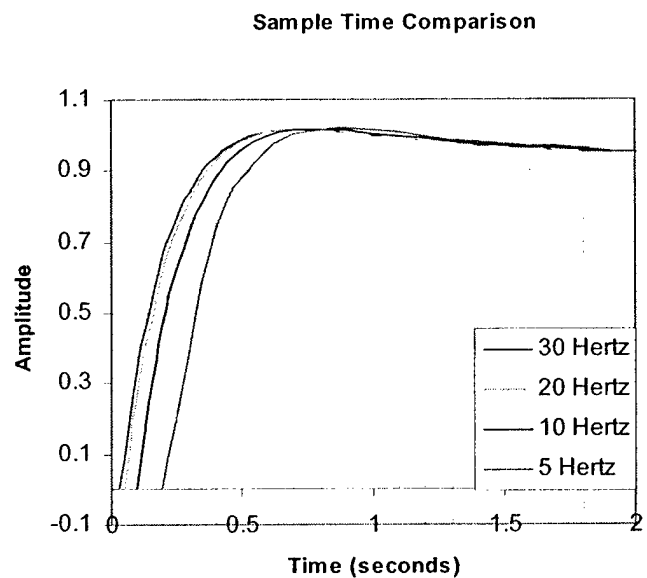


Figure 5.1 Lagging Effects Associated with Sample Time

variety of sampling rates. The first step was to map the discrete system from the continuous system using the most accurate method available (Messner)

$$z = e^{Ts}$$

This method however does not work with PID because the discrete transfer function would have more zeros than poles. A modified method that will allow mapping from continuous to discrete system is known as the Bilinear Transformation (Xu). The transformation maps the entire left hand side of the s-domain into a unit circle in the z-domain. This transformation introduces sample time ( $T_s$ ) to get a function in the z-domain. The relationship between the s-domain and the z-domain is as follows

$$s = \frac{2}{T_s} \frac{z-1}{z+1}$$

When the value of s is substituted into the continuous PID transfer function, the equation becomes

$$K_p + \frac{K_i T_s}{2} \left( \frac{z+1}{z-1} \right) + \frac{K_d}{T_s} 2 \left( \frac{z-1}{z+1} \right)$$

Now the discrete system can be tuned according to the current sample rate. The discrete transfer function of the system for PID control becomes

$$\frac{X(z)}{F(z)} = \frac{(K_p + K_i T_s + \frac{2K_d}{T_s})z^2 + (K_i T_s - \frac{4K_d}{T_s})z + (-K_p + \frac{K_i T_s}{2} + \frac{2K_d}{T_s})}{z^2 - 1}$$

To better understand the effect of sample rate on the gain scheduling, gain terms in the equations above were isolated and plotted to find an algorithm to scale the gains within the code. Figure 5.2 shows a very simple relationship between

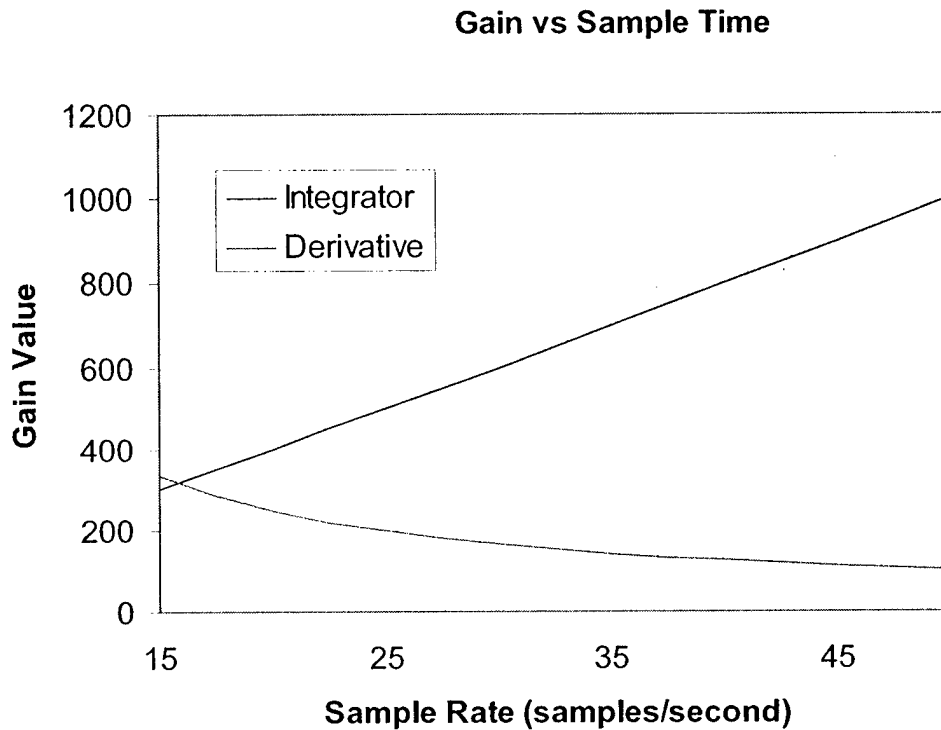


Figure 5.2 Gain Variation with Sample Time

sample time and gain. The proportional gain is unaffected by sample rate. The equation of the integrator term that would be implemented into the code is the curve fit to the line shown in Figure 5.2. The equation is as follows:

$$K_I = 20 * T_s$$

Likewise, the derivative term is

$$K_D = 0.207 * T_s^2 - 19.63 * T_s + 570$$

where  $T_S$  is the sample time. With these relationships, the gains can be varied as the system requires maintaining optimal performance.

## **6 Experimental Setup and Procedure**

The experimental testing of the active control scheme on the wind tunnel model entailed several separate systems working together. These systems include: wind tunnel, data acquisition, the driving system and the active control system.

### ***6.1 Wind Tunnel***

The main facility used for the experiment is California Polytechnic State University's 3'x4' wind tunnel located in the Aero Hanger on campus in San Luis Obispo, California. The wind tunnel is known for very clean, steady flow in the test section and is very easy to operate with a digital control system. Figure 6.1 illustrates the top-view geometry of the wind tunnel and the control room.

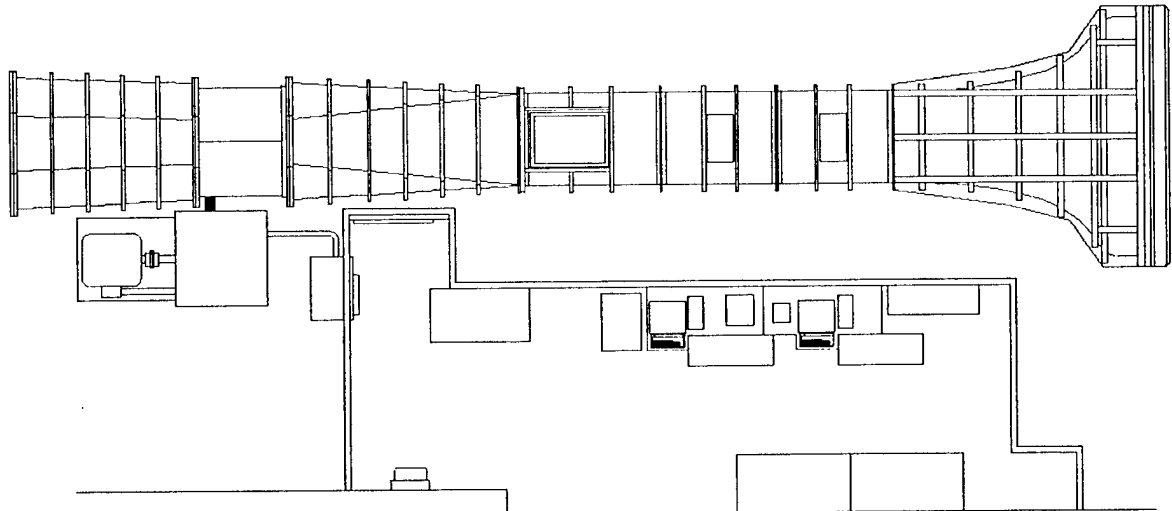


Figure 6.1 Wind Tunnel

## **6.2 Data Acquisition**

To evaluate the effectiveness of the active control system, a LabView program was written by a former graduate student (Wait) to record data from on-board sensors on the aircraft. The main sensor is a Murata ENC-05EB piezo rate gyro located in the nose of the aircraft, approximately where a pilot would fly the airplane. The data acquisition system starts with a GUI that displays the gyro output versus time on an easy-to-read graph. A second graph illustrates the input force versus time to verify the accuracy of the input. The user has the capability of taking the data at any time for storage in a Microsoft Excel file. The data can then be used to generate performance plots for comparison, as will be shown in section 7. Refer to Figure 6.2 for an illustration of the LabView interface.

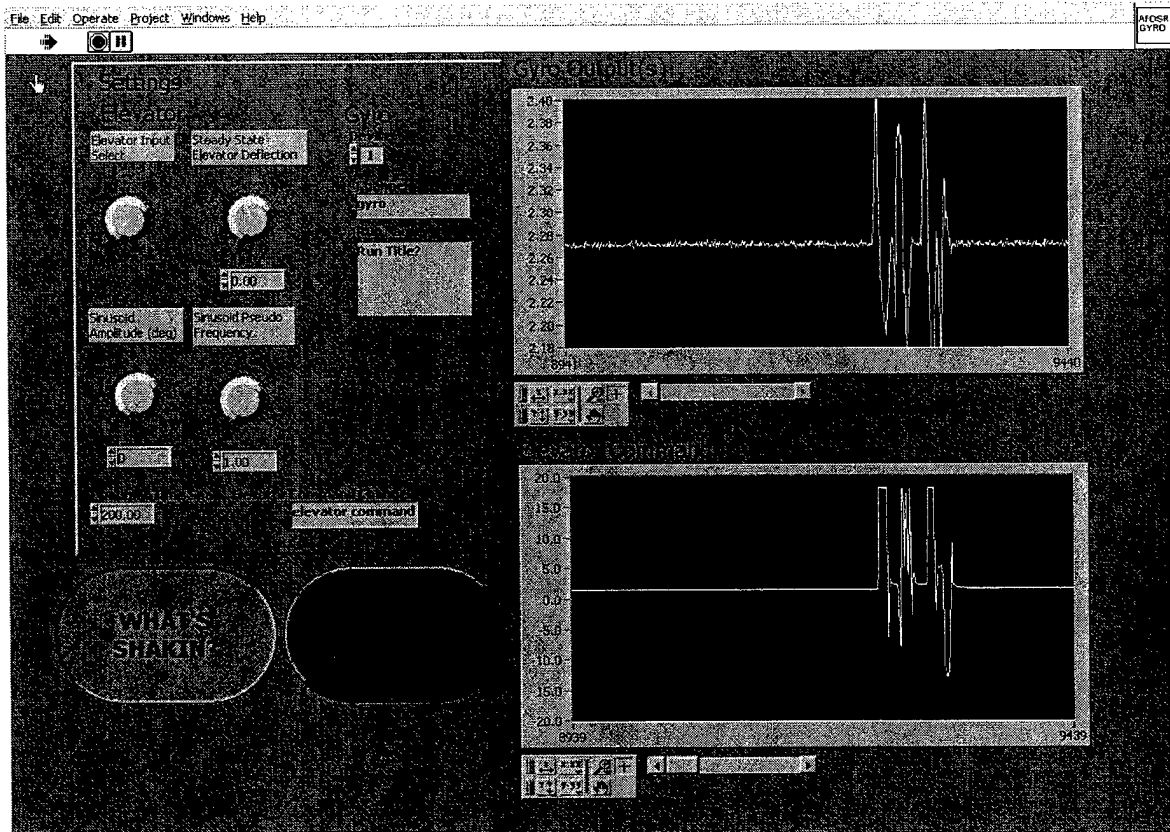


Figure 6.2 LabView GUI

### 6.3 Driving System

Originally, the natural frequency of the vehicle was to be excited by a turbulence generator upstream. However, due to the natural damping of the vehicle with a constant down force provided by the horizontal tail, another method was explored to excite the structural modes. By running a servo on the elevator of the aircraft, LabView could control the input at a desired frequency and amplitude. The servo is a Hitech HS-50 with a maximum bandwidth of 50 hertz and a weight of 0.2 ounces. The setup allowed the user to instantly change

the waveform for optimal excitation. Ultimately, the first bending mode was excited with a sinusoidal input from the servo.

#### 6.4 Active Control Architecture

The experimental setup for the active control system includes all of the hardware required to both sense and increase the response of the tail boom. There are strain gages and actuators located at 2 locations on the top and bottom of the tail boom. Figure 6.3 illustrates the signal flow. The wiring is concealed in a shrink-wrapped wiring harness that extends from the vehicle to

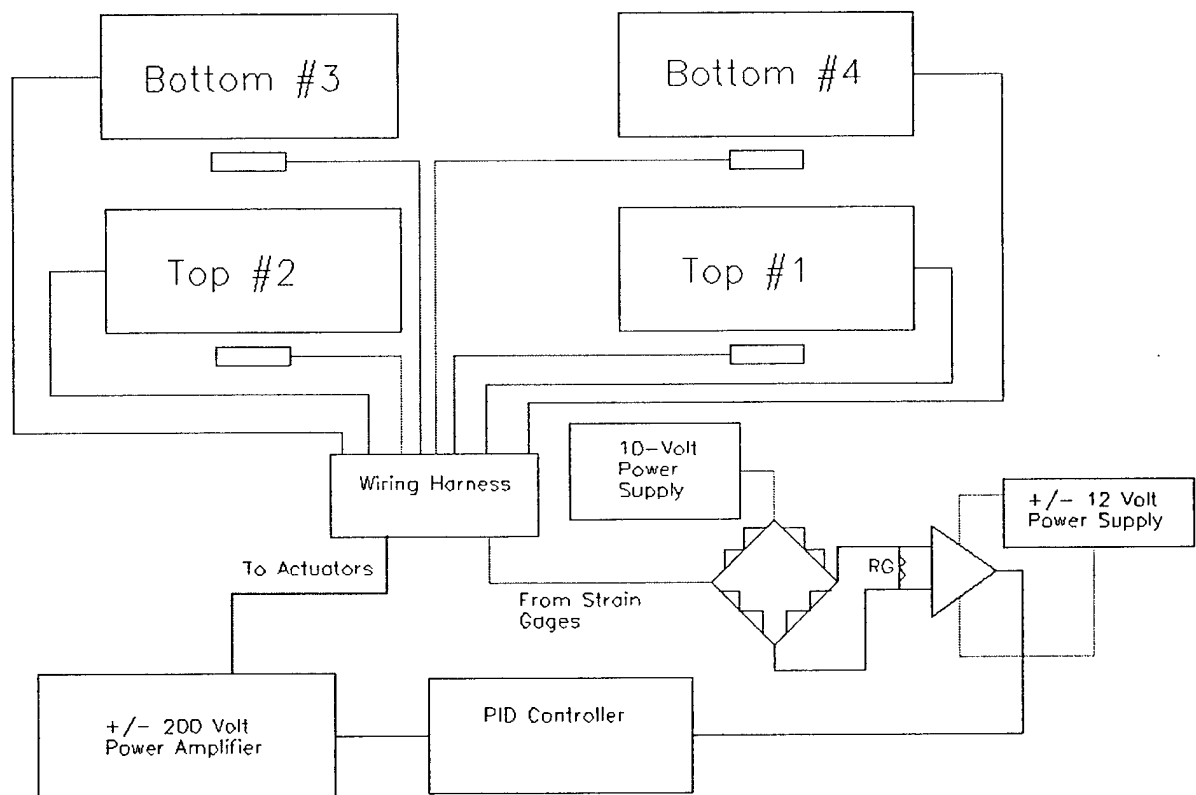


Figure 6.3 Active Control Signal Diagram

the rest of the hardware located outside the wind tunnel. The signal flows from the actuators, through the wiring harness into the full bridge circuit. The full



bridge circuit is supplied by a 10-volt power source that amplifies the signal before feeding into the instrumentation amplifier (INA-122). The op-amp is powered by a +/- 12-volt power supply made by DigiKey Corporation. The PID controller filters the signal before outputting to the power amplifier constructed by Mark Kettering, a former Cal Poly graduate student. The high-voltage output from the power amp goes directly to the ACX actuators.

## **6.5 Experimental Procedure**

Once the hardware is functioning properly, the wind tunnel is turned on to provide 30 feet per second flow in the test section. The speed of the flow was optimized to provide the best performance of the active control system. LabView is then initialized to acquire data and the input signal is sent to the servo. The aircraft is constrained to move only about the pitch axis with a hyme joint. The airplane pitches up and down at a frequency determined real-time by the LabView interface. Data from the gyro in the nose of the aircraft is logged and plotted to determine the performance of the system. The variables in the procedure include; wind tunnel speed, driving frequency, amplitude and waveform.

### **6.5.0 Wind Tunnel Velocity**

The speed of the flow in the test section determined the steady-state deflection of the beam. As the speed increased, the tail boom deflection increased until the "tucking" occurred. The tucking was unavoidable because the

actuators did not have enough power at high wind tunnel speeds to prevent the tail boom from bending. There was also a minimum speed requirement to keep the airplane flying. With the servo driving the deflection, a sweep of wind tunnel speeds was performed to find the optimal speed for the active control system. At very high speeds, the natural damping of the tail masked test data by preventing overshoots that would have naturally occurred at lower speeds. At very low speeds, the airplane would not fly. The final speed that produced the best data was 30 feet per second.

#### *6.5.1 Driving Signal Characteristics*

The waveform, frequency, and amplitude were all varied to give optimal test results. The waveform that simulated a pilot's input while maneuvering is a step input. This was the worst-case scenario with respect to the active system output requirements. Sinusoidal and saw tooth were also input for observation, but the square step input yielded the best data. The frequency was varied in an attempt to excite the natural mode of the tail boom. However, the damping provided by the tail would never allow the natural modes to emerge in the data. For this reason, the frequency was kept at the design frequency of 2 hertz. A sweep of various amplitudes was not initially performed until the data was carefully reduced. The first plots show the data has a lot of noise that once filtered, reduces the apparent performance of the active system. Figure 6.4 illustrates the noisy output from the gyro for several different gain values.

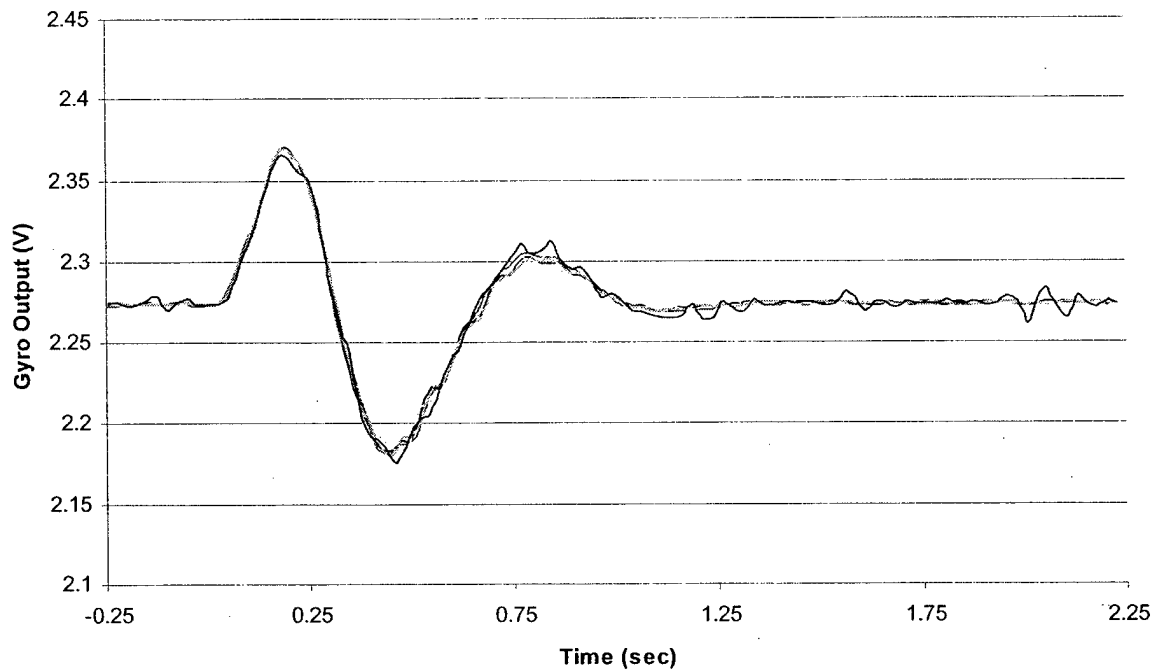


Figure 6.4 Unfiltered Output

After initial tests, a filter in LabView was introduced to reduce the noise. Due to the decrease in signal strength from the filtering, the amplitude was maximized in an effort to provide useful data. Figure 6.5 shows the filtered signal for two runs: one run with the active system on and the other with the active system off. The amplitude was increased until the sting balance and the roof of the wind tunnel were close to interfering with the movement of the aircraft.

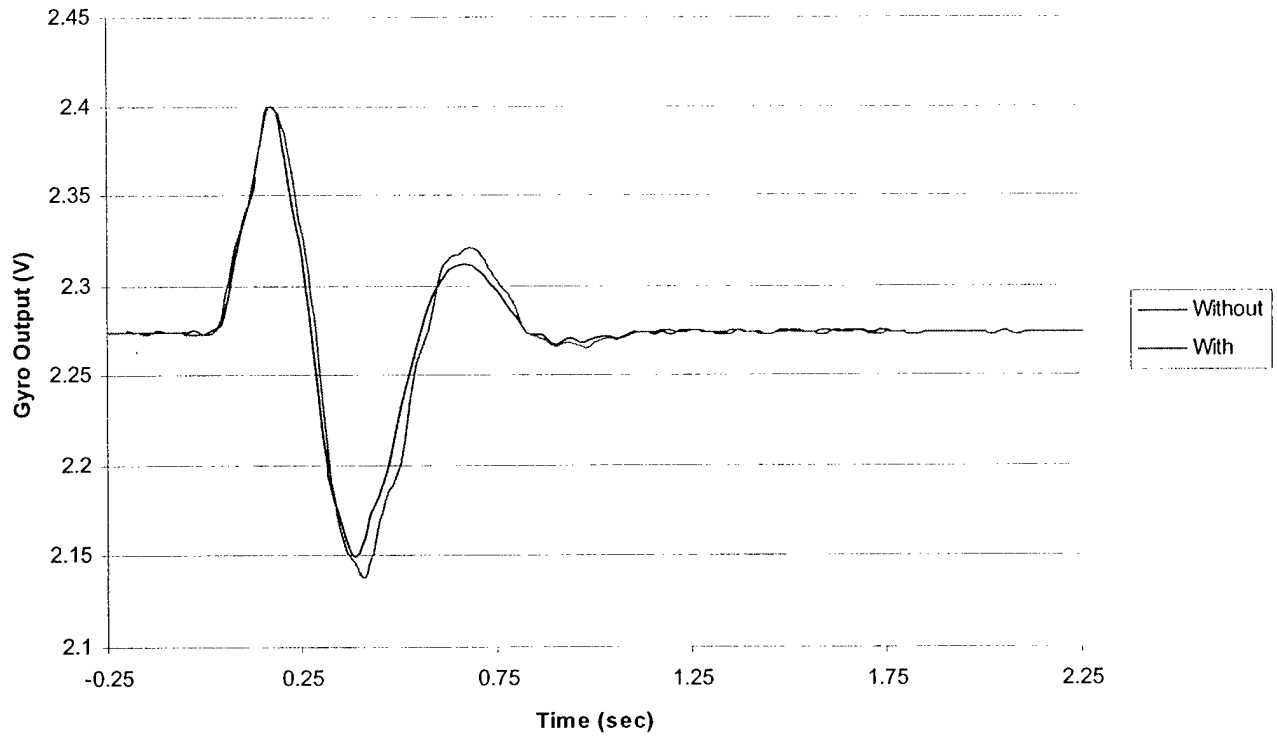


Figure 6.5 Filtered Output

## 7 Results

Once the testing was complete, the data was reduced to find the optimal gain schedule for the active control system. A series of tests were performed with a variety of gain schedules to determine the best gains for the system. Figure 7.1 illustrates the schedule for varying the gains. The effect of each

Run Number	Proportional	Integral	Derivative
1	5	0	0
2	10	0	5
3	10	2	5
4	20	0	8

Figure 7.1 Gain Schedules

separate gain schedule was very difficult to determine for all the runs except run three, where the integrator term was nonzero. For any nonzero value of the integrator term, the system would oscillate at its natural frequency. The phase shift introduced by the integrator caused the system to go unstable. For this reason, the integrator term was kept at zero.

The performance of the active control system was determined by recording the output with the system on, and without the system on. Figure 7.2 illustrates the

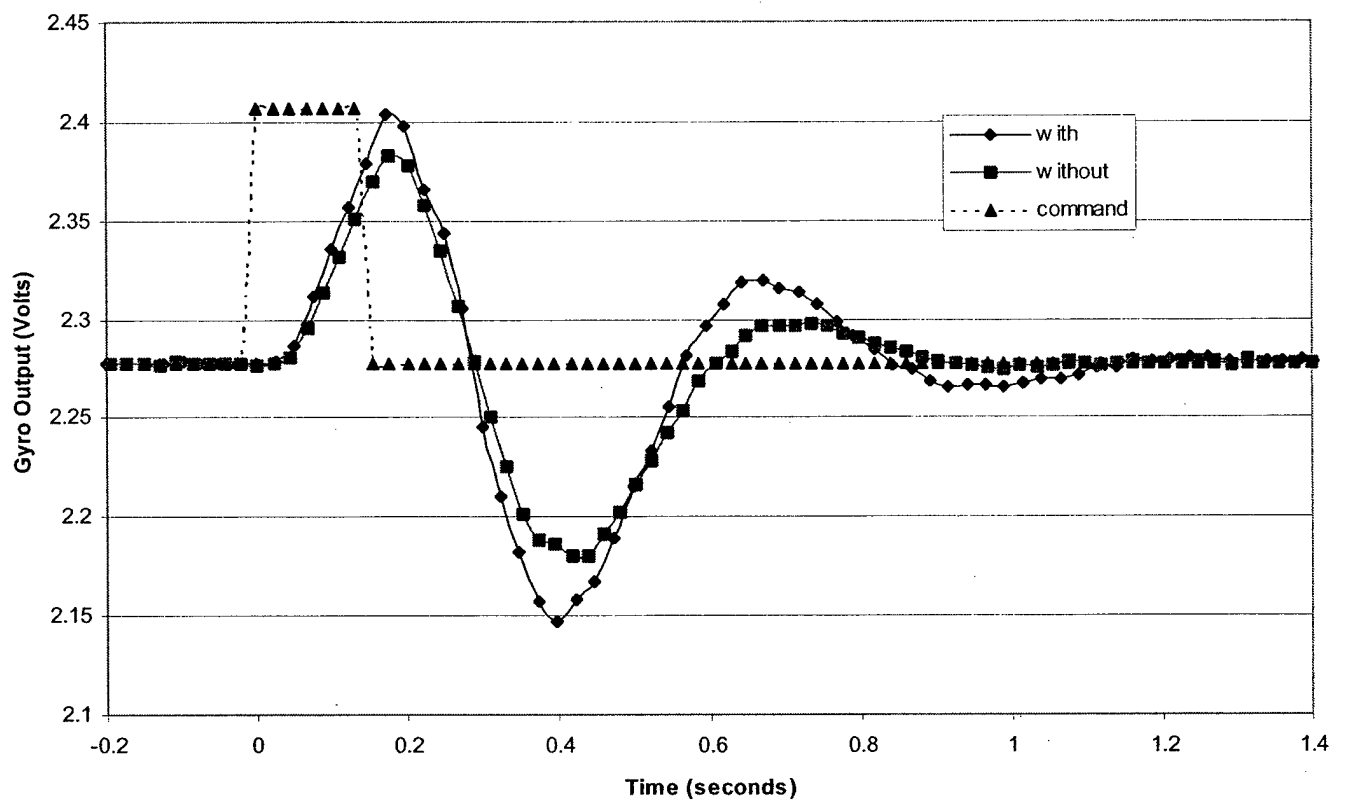


Figure 7.2 Gyro Output

results from the testing. At first glance, the results seem non-intuitive. The active system displays more overshoot than the uncompensated system. The

active system is physically making the fuselage more rigid, therefore increasing its ability to respond to an input. The higher maximum and minimum values shown in Figure 7.2 are a result of an increase in pitch rate that the active system provided.

The actual pitch rate was calculated using the gyro scale factor of 0.67 mV/°/second, given by the manufacturer. The results, illustrated in Figure 7.3, show the pitch rate was increased by 19% with the active control system on.

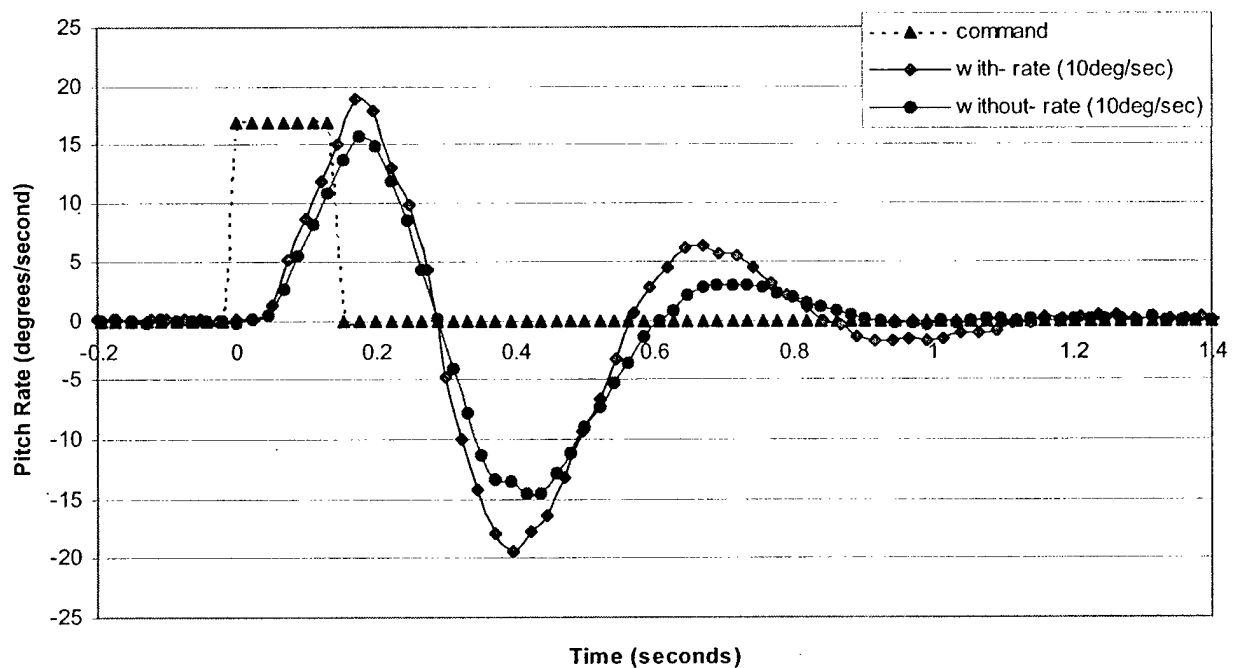


Figure 7.3 Pitch Rate Comparison

Notice the steady-state error that remains because the integrator gain is set to zero.

Further reduction of the data was done to investigate the pitch angle response with the active control system. Figure 7.4 shows the tremendous improvement in both magnitude and response time for the system. There is a 21% increase in

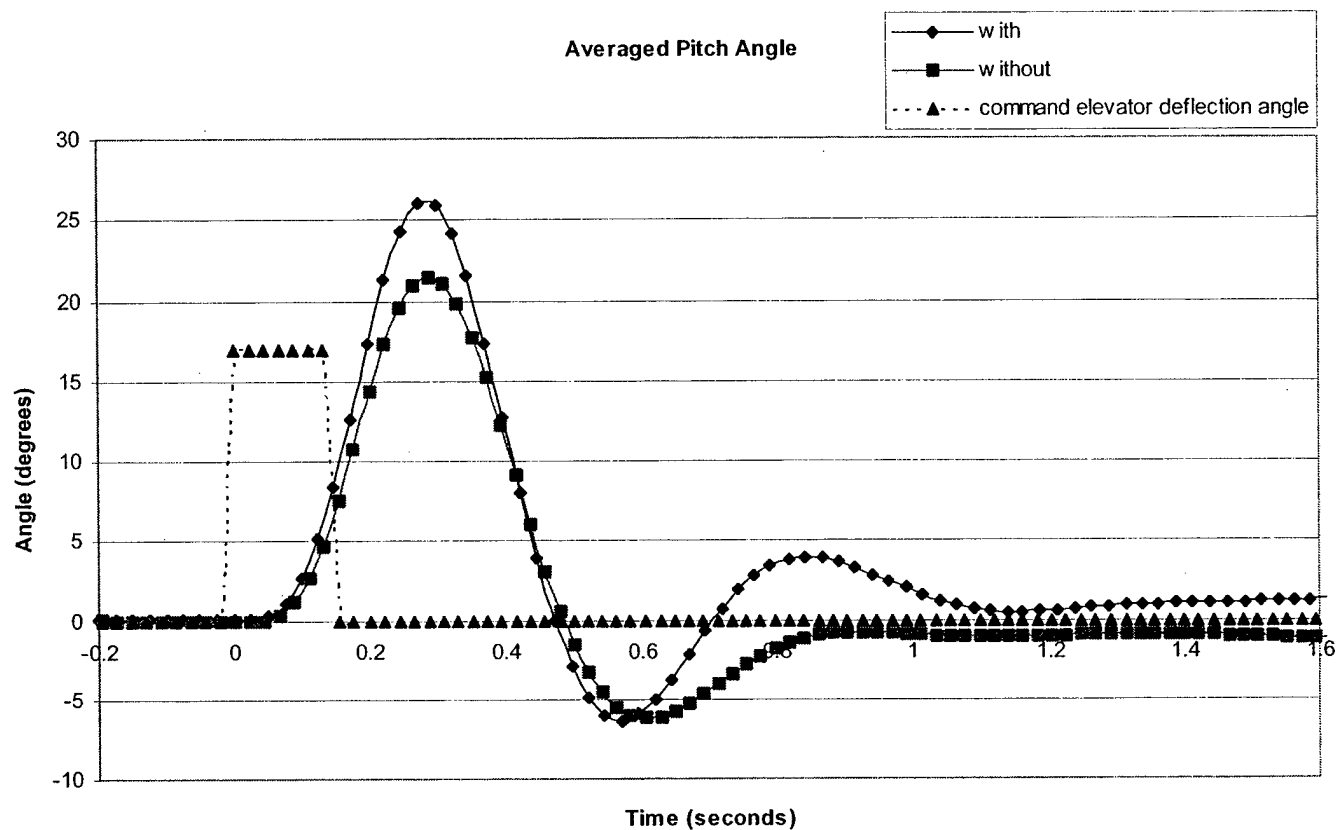


Figure 7.4 Pitch Angle Performance

total pitch angle with the active control system on. Additionally, the response time was increased by 22%. The response time was measured from the time between zero command and maximum angle achieved of 21 degrees.

## 8 Conclusion

The effects of active control can be utilized for a wide range of applications. The primary goal of this research was to investigate a method for removing system lag due to an unstable structure. The preceding work has revealed the destabilizing effect of a non-rigid structure can be removed by implementing an active control system with a digital PID control loop.

The results show the active control system greatly improved overall performance. The pitch response was increased by 21% and the maximum achievable pitch angle was increased by 22%. These results are magnified by the construction techniques of the aircraft. For implementation on a full-scale airframe, the overall performance could be less apparent. However, when handling qualities are considered, the implementation of active control is highly recommended if the airframe is flexible.



## 9 References

- 1 Active Control eXperts "Piezoceramic Actuator, A Division of Cymer."  
1994. [www.acx.com](http://www.acx.com) (10 April 2000).
- 2 Hashii, W. N., Munger, A. R., Elghandour, E., Kolkailah, F. A., & Biezd, D. J. Investigation of dynamic structural models suitable for the simulation of large aircraft. AIAA Paper 99-4320 *Proc. Of the AIAA Modeling and Simulation Technologies Conf. and Exhibit* Collection of Technical Papers (A99-36794 09-54). 1999.
- 3 Messner, Bill & Tilbury, Dawn "Controls Tutorials for Matlab." Carnegie Mellon University. 1997 <http://www.engin.umich.edu/group/ctm/> (20 January 2001).
- 4 Munger, A. R., Hashii, W. N., Elghandour, E., Kolkailah, F. A., & Biezd, D. J. Transfer functions for simulating the structural vibration modes of large aircraft. AIAA Paper 99-4108 *Proc. Of the AIAA Atmospheric Flight Mechanics Conf. and Exhibit* Collection of Technical Papers (A99-36864 09-0) 1999.
- 5 Nise, Norman S. Control Systems Engineering. Menlo Park, CA: Addison-Wesley Publishing Company, 1995.
- 6 Powers, B. G. Structural Dynamic Model Obtained from Flight for Use with Piloted Simulation and Handling Qualities Analysis. NASA TM 4747, 1996.
- 7 Smith, J. W., & Berry, Donald T. Analysis of Longitudinal Pilot-Induced Oscillation Tendencies of YF-12 Aircraft. NASA TN D-7900, 1975.

- 8 Xu, Hao, Aniruddha Datta, and S.P. Bhattacharyya. "Computation of All Stabilizing PID Gains for Digital Control Systems." Automatic Control April (2001): Volume 46.
- 9 Wait, Daniel. "Design and Implementation of a Dynamic Measurement System for Cal Poly Low Speed Wind Tunnel." Thesis. California Polytechnic State University, 2001.